Scoping the characteristics and benefits of a connected double-null configuration for power exhaust in EU-DEMO

Nuclear Materials and Energy 26 (2021) 100886

Contents lists available at ScienceDirect

Nuclear Materials and Energy

journal homepage: www.elsevier.com/locate/nme

Scoping the characteristics and benefits of a connected double-null configuration for power exhaust in EU-DEMO

L. Aho-Mantila [a,*], F. Subba [b], D.P. Coster [c], L. Xiang [d], F. Militello [d], T. Lunt [c], D. Moulton [d], H. Reimerdes [e], M. Wensing [e], M. Wischmeier [c], R. Ambrosino [f], X. Bonnin [g], M. Siccinio [h,c]

[a] VTT Technical Research Centre of Finland, FI-02044 VTT, Finland
[b] NEMO Group, Politecnico di Torino, Corso Duca degli Abruzzi 24, 10129 Torino, Italy
[c] Max-Planck Institut für Plasmaphysik, D-85748 Garching, Germany
[d] CCFE – UKAEA, Culham Science Centre, Abingdon OX14 3DB, UK
[e] Ecole Polytechnique Fédérale de Lausanne (EPFL), Swiss Plasma Center (SPC), CH-1015 Lausanne, Switzerland
[f] C.R.E.A.T.E. Consortium, ENEA, Napoli, Italy
[g] ITER Organization, Route de Vinon-sur-Verdon, CS 90046, 13067 St Paul-lez-Durance Cedex, France
[h] Eurofusion PMU, Boltzmannstrasse 2, D-85748 Garching, Germany

ARTICLE INFO

Keywords:
DEMO
Power exhaust
SOLPS-ITER
Double-null
Divertor physics
Operating space

ABSTRACT

A double-null configuration is being considered for the EU-DEMO, due to its potential benefits for power exhaust arising from the use of two active divertors and magnetically disconnected low- and high-field sides. Using systematic parameter scans in fluid simulations, we have investigated the divertor power exhaust in the EU-DEMO in a connected double-null configuration, and compared the edge plasma properties to those obtained in a single-null configuration under detached conditions anticipated for reactor operation. Neglecting drift effects and kinetic behaviour of the neutrals, no clear benefits of the double-null configuration could yet be identified for the radiation pattern and power mitigation on open field lines. Future work should address the aforementioned physics as well as the effect of the additional X-point on core radiation.

1. Introduction

The presently foreseen power exhaust solution for the EU-DEMO is based on an ITER-like single-null (SN) configuration, with metallic walls and impurities seeded into the plasma edge to mitigate the divertor heat fluxes. This strategy requires a carefully optimized mix of seed impurities and, depending on the width of the radial heat flux profile in the scrape-off layer (SOL), more than 90% of the plasma power may need to be dissipated before it reaches the walls. In addition to this, high upstream density may be required to enhance the divertor power losses and facilitate detachment which, combined with the density limit for the confined plasma, may lead to a very narrow suitable operating space, or no operating space at all. Even if possible operating points can be found, they must be compatible with a feasible plasma scenario and form a window that is large enough to accommodate small imperfections in the control and suppression of transients, and allow for the unavoidable steady-state fluctuations in the plasma.

As a risk mitigation strategy, several alternative divertor configurations (ADCs) are being considered for the power exhaust solution in the EU-DEMO, aiming to increase the wetted area, enhance the heat flux mitigation, or stabilize the radiation fronts to allow for a larger operating window [1,2]. In this contribution, we study the power exhaust characteristics of a connected double-null (DN) configuration, which uses two active divertors, but has no magnetic field lines in the main SOL that connect the inboard and outboard sides. The modelling is done using fluid simulations with reduced physics models designed for reactor scoping studies [3], enabling a systematic parameter scan for exploring the characteristics of this configuration on a reactor scale. Although some of the excluded physics (e.g. cross-field drifts, kinetic behaviour of neutrals) could influence the solutions or at least the quantitative results obtained, their inclusion in the simulations is computationally too demanding for the large parameter scans carried out for this work. With our present approach, we identify the main characteristics and exhaust regimes in the DN configuration, which will serve as a basis for designing more detailed physics studies, if estimated necessary. Furthermore, we perform a comparative study between the

* Corresponding author at: P.O. Box 1000, FI-02044 VTT, Finland.
E-mail address: leena.aho-mantila@vtt.fi (L. Aho-Mantila).

https://doi.org/10.1016/j.nme.2020.100886
Received 31 July 2020; Received in revised form 18 November 2020; Accepted 8 December 2020
Available online 21 January 2021

baseline SN and the DN configuration which, even when using reduced physics models, could help identifying if one of the configurations has major benefits compared to the other.

2. Modelling assumptions

A connected DN configuration is studied as a possible alternative solution to the EU-DEMO SN configuration. The engineering design is based on the baseline DEMO1 SN solution, although certain advanced features that have been optimized for the SN configuration have been excluded in the (2018) designs studied here [2]. The triangularity and elongation is kept similar between the two configurations, and the plasma volumes are nearly identical (1.5% smaller in DN). The connection lengths from the midplane to the targets, L, and the flux expansions at the targets, f, are shown in Figs. 1 and 2 for a flux surface near the separatrix ($\Delta R_{\mathrm{midplane}} \sim 1$ mm). The magnetic field incidence angle at the targets is 1.5°. The two X-points in the DN configuration are located at equal distances from the $R = 0$ and $z = 0$ axes, such that the configuration is as symmetric as possible, although with small deviations in the connection lengths as shown in Fig. 1.

The simulations are set up to model power exhaust in the SOL and divertors, excluding specific core radiators. Because of the uncertainties involved in the transport and core plasma properties, technical solutions and engineering limits, the detailed modelling assumptions described here may need to be revised for future studies. However, they are estimated sufficiently accurate for the purpose of the qualitative and comparative studies presented in this paper. It is assumed that from the 450 MW of power carried by the plasma, 300 MW can be radiated inside the core, corresponding to a core radiated power fraction $f_{\mathrm{rad,core}} = 67\%$ and leaving 150 MW to enter the SOL. For the scrape-off layer heat flux width, λ_q, diffusivities yielding $\lambda_q \sim 3$ mm are assumed. This value of λ_q is largerthan what some of the most critical estimates may give, but a practical choice within the range of possible projections to DEMO [1] to ease the numerical treatment and allow for a first comparison of the effects of the divertor configuration. The seeded impurity is taken to be Ar, which in present devices radiates partly on closed field lines but in DEMO is expected to be more a divertor radiator. The target safety limits are taken to be peak electron temperature $T_{\mathrm{e,pk}} < 5$ eV and peak heat flux $q_{\mathrm{pk}} < 10$ MW/m^2, of which the first approximates a satisfactory low level of W sputtering and the latter will ultimately depend on the material composition of the target PFCs (the limit may be lower). The upstream density limit is set to 60% of the Greenwald density, n_{GW} (7.0×10^{19} m^{-3}), at the outer midplane separatrix, acknowledging that also this limit may ultimately be lower.

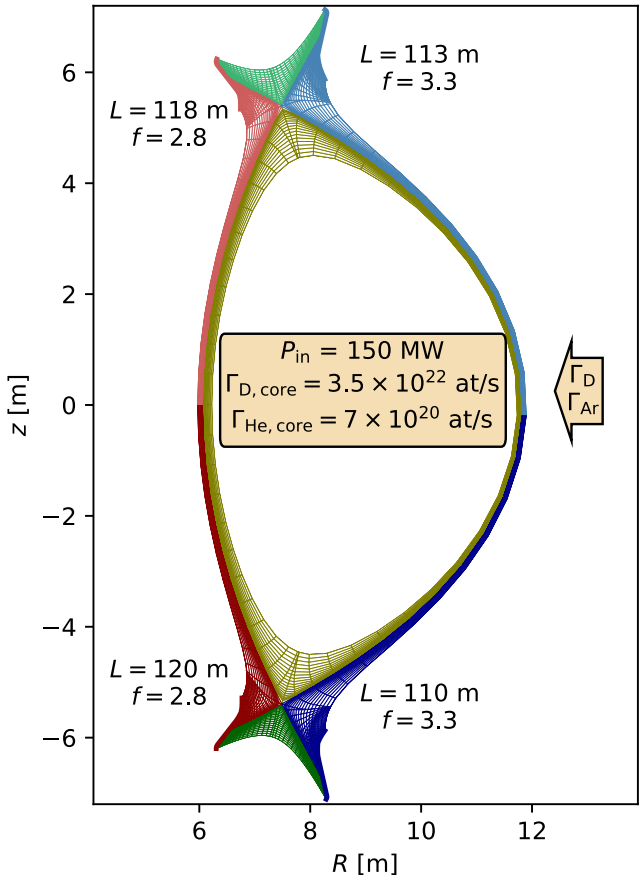

Fig. 1. Computational mesh used for simulating the EU-DEMO DN configuration, having 144 (+4) grid points in the poloidal direction and 36 (+2) grid points in the radial direction (+ guard cells). The various plasma regions are highlighted with the same colours that are used in Section 3.1 to plot the simulation results.

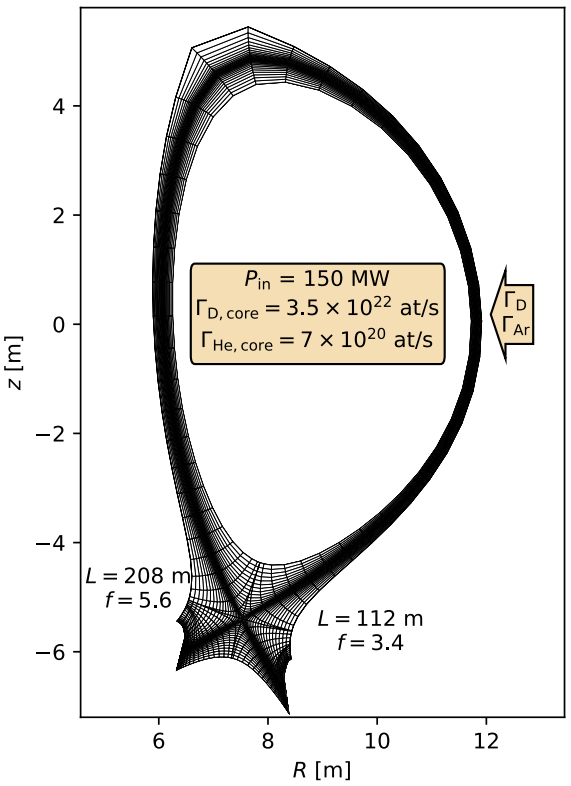

Fig. 2. Computational mesh used for simulating the EU-DEMO SN configuration, having 96 (+2) grid points in the poloidal direction and 36 (+2) grid points in the radial direction (+ guard cells).

The B2.5 computational meshes created for the SOLPS-ITER [4,5] (fluid neutral) simulations are shown in Figs. 1 and 2 together with the key input particle and power fluxes (the input power is shared equally between the electrons and ions). The fuelling and impurity seeding are implemented with variable strengths on the outboard side, and 1% of the neutrals are absorbed on the private-flux region (PFR) boundaries, representing pumping in both upper and lower divertor. The latter is a simplification in the absence of a more detailed pumping model, which would be needed if kinetic neutrals would be followed. The general simulation settings are the same for all of the 2018 ADCs, which are being modelled with SOLPS-ITER [2]. Radial transport is described by a constant particle diffusion coefficient ($D_\perp = 0.1$ m^2/s) and viscosity (0.2 m^2/s), whereas the heat diffusion coefficients (χ_e, χ_i) are specified to increase in the pedestal region ($\Delta R_{\mathrm{midplane}} = [-5$ mm, 0 mm]) from the core values (0.1 m^2/s) to the SOL values (0.3 m^2/s). Flux limiters are in use for the electron heat (0.2), viscosity (0.375), and thermal and friction forces (0.5). A flux limiter for the fluid neutrals is used as

recommended in [6] and Ar is bundled into 3 charge states as in [3]. The intrinsic species are simplified to be D (no explicit treatment of T) and He (neglecting small levels of other intrinsic impurities). All the cases shown in the present paper have cross-field drift terms deactivated.

3. Results

3.1. Radiation pattern and detachment in DN

We first describe the variation in the SOL conditions, when variable levels of Ar seeding are imposed while keeping the separatrix plasma density at the outboard midplane, $n_{sep,omp}$, constant by operating the D gas puff in a feedback mode. This parameter scan aims to characterize the power exhaust processes under as constant upstream conditions as possible. Section 3.2 investigates how the impurity seeding modifies the upstream conditions in more detail.

Fig. 3 shows the evolution of the simulated radiated power fraction, P_{rad}/P_{in}, where $P_{in} = 150$ MW, with increasing Ar seeding level. Only D and Ar contribute non-negligible amounts to the total radiated power, and less than 3% of the radiation originates from closed field lines, such that $f_{rad,SOL}$ can be approximated to be equal to the total value indicated by the dashed line. In Fig. 4, the resulting peak power loads and target temperatures are shown, whereas Fig. 5 shows the heat fluxes entering the divertor legs (at the X-point locations) and the enrichment of Ar in the divertor legs compared to the upstream SOL (these two regions are separated from each other at the X-point location). For calculation of the enrichment, n_{Ar}/n_D is evaluated upstream as an average on the first SOL ring, and in the divertor as an average over all the cells that are within 3 mm radial distance from the separatrix, when mapped to the midplane.

The radiation pattern and divertor conditions are observed to evolve as follows:

- At the lowest seeding levels, $f_{rad,SOL} < 35\%$ and $\Gamma_{Ar} < 10^{20}$ s^{-1}, an up-down asymmetry emerges and becomes larger with increasing seeding, as most of the radiation increase takes place in the upper divertor, whereas an increase of heat fluxes to the lower divertor is observed. Both q_{pk} and $T_{e,pk}$ decrease below the safety limits in the upper divertor, whereas an increase in these parameters is observed in the lower divertor. Ar enrichment becomes larger in the upper divertor. In the lower divertor, q_{pk} and $T_{e,pk}$ have an in-out asymmetry with higher values obtained in the outer divertor, but these parameters become symmetric as $f_{rad,SOL}$ increases above 20%. At $f_{rad,SOL} > 20\%$, the initially symmetric q_{pk} in the upper divertor becomes asymmetric, with higher values obtained on the outboard side.
- At higher seeding levels, $35\% < f_{rad,SOL} < 60\%$ and 10^{20} s$^{-1} < \Gamma_{Ar} < 4 \times 10^{20}$ s^{-1}, the lower divertor begins to cool down, with $T_{e,pk}$ and q_{pk} reducing first at the lower outer target and later at the lower inner target. The radiation increase is, however, taken up primarily by the upper divertor, particularly by the upper outer SOL. The heat fluxes entering the upper divertor increase. The conditions are not yet suitable for operation, due to the high target temperatures in the lower divertor.
- Strong radiation in the lower divertor is obtained only at the highest seeding levels, $f_{rad,SOL} \sim 70$ % and $\Gamma_{Ar} \geqslant 4 \times 10^{20}$ s^{-1}. Up-down

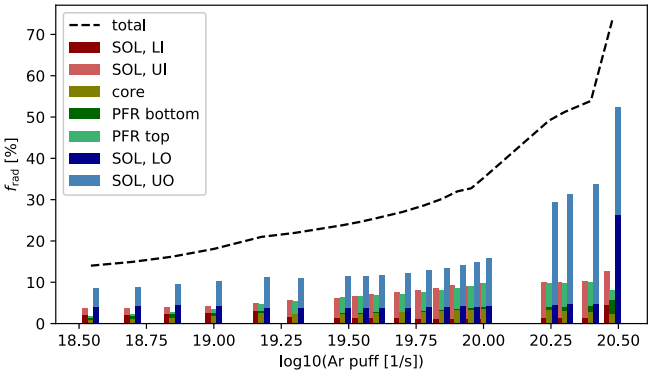

Fig. 3. Radiated power fractions, P_{rad}/P_{in}, when P_{rad} is evaluated in the different regions described in the legend ("LO" = lower outer, "LI" = lower inner, "UO" = upper outer, "UI" = upper inner), see also Fig. 1. The dashed line gives f_{rad} when radiation in the entire simulation volume is taken into account. On the x-axis, we have chosen to give the logarithm of the Ar puff rate, as this provides the best visualization of the various exhaust regimes. A value X corresponds to 10^X at/s Ar seeding.

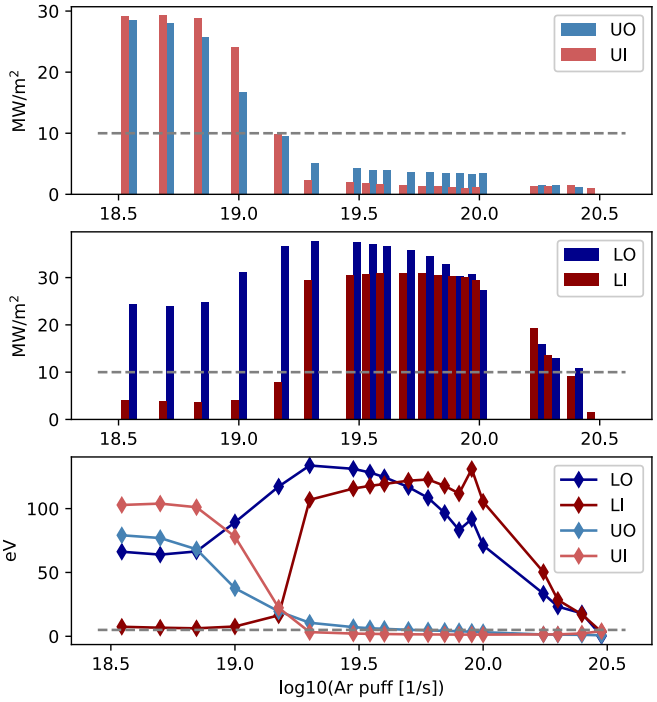

Fig. 4. Peak heat loads (bars) and temperatures (solid lines with diamonds) at the targets, labelled as in Fig. 3. The dashed grey lines indicate the ope. rational limits.

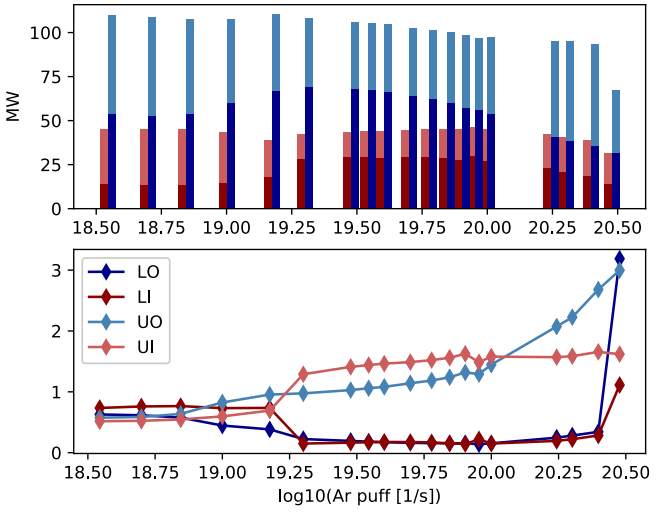

Fig. 5. Heat fluxes entering the divertor regions (upper figure) and Ar enrichment in the divertor legs (lower figure). The colour coding is the same for both plots.

asymmetries are small and the in-out asymmetry in the radiated power fractions is close to the level expected due to geometric reasons. The heat loads and target temperatures are mitigated to acceptable levels on all targets.

The asymmetries observed in the evolution of the divertor conditions can be understood as follows. At low seeding levels or in the absence of external impurities, the total heat fluxes entering the inboard and outboard divertors have an asymmetry as expected by the in-out asymmetry of the flux surface areas. The midplane separatrix density is also a few percent higher on the outboard side. Conduction carries nearly all of the heat to the divertors which, in the absence of currents, would lead to nearly up-down symmetric target conditions. The symmetry is not perfect, however, due to small inherent imperfections in the symmetry of the computational mesh, which result in a small temperature asymmetry between the upper and lower targets (ΔT_e = 5–20 eV in the absence of currents). This observation is consistent with the conclusions made previously from B2.5-SOLPS modelling of MAST Upgrade CDN discharges [7]. The temperature difference gives rise to thermoelectric currents, which are associated with heat flow from the colder to the hotter target, reinforcing the temperature difference between the lower and the upper targets, separately for each side of the plasma. On the inboard side, the effect of the currents is large enough to bring the lower inner divertor from a low collisionality regime ($\lambda_{T_e} = T_e^2/n_e \times 10^{16} > 10$ m) to a more collisional regime ($\lambda_{T_e} < 1$ m), in which strong temperature gradients can be sustained, resulting in a significant cooling of the lower inner target. On the outboard side, which in the absence of currents has a smaller up-down ΔT_e than the inboard side, the effect of the currents is not large enough for significant cooling of either of the targets.

When Ar is injected into the plasma, the radiative power losses become largest in those plasma regions, which are the coolest (but still dense enough). This is due to the temperature dependence of the radiative losses of Ar, which has a maximum at a few dozen eV, significantly below the peak target temperatures. On the inboard side, the coolest temperatures are obtained in the lower divertor leg. However, the lower inner divertor leg receives only about 10% of the SOL input power, so even with efficient radiation it cannot contribute much to the total radiated power fraction. On the outboard side, the power fluxes are larger, and the radiative losses become soon largest in the cooler upper divertor leg. As the upper outer target transitions to a high-recycling regime, the Ar neutrals residing in the far SOL of the divertor leg are able to travel closer to the strike point, and the Ar concentration and enrichment increase in the upper outer divertor. The radiated power losses increase, cooling the target further. Finally, more Ar is able to penetrate into the PFR region and to the inboard divertor leg, increasing the radiation losses also on the inboard side. The cooling of the upper divertor leads to a reversal of the thermoelectric currents, more heat is transported to the lower divertor, and the lower divertor peak temperatures increase. This results in the strong up-down asymmetries observed at Ar seeding levels 10^{19} s^{-1}–10^{20} s^{-1} in Figs. 4 and 5, with a cooler and more radiating plasma in the upper divertor compared to the lower divertor.

When even more Ar is injected into the plasma, a similar process takes place in the lower divertor: Ar densities begin to increase in the lower outer divertor, first in the far SOL regions. This results in a similar cooling, increase of impurity density, and increasing radiation as in the upper divertor, resulting in a complete cooling down and detachment of the lower outer divertor plasma. Similar to the upper divertor, also in the lower divertor the inner target begins to cool down slightly later than the outer target, due to impurities travelling from the outer target through the lower PFR to the inner target first. The detachment is deeper on the outboard side, which has higher neutral densities. A small level of up-down asymmetry remains as the impurity densities are lower in the lower inner divertor leg compared to the upper inner divertor leg.

Finally, it should be noted that both the direction of the currents and the impurity radiation pattern are dependent on the plasma temperature and density profiles, and the initial conditions can influence the outcome of the simulations. We see this in the case of strongly asymmetric conditions, where a plasma state, which is reversed in the up-down direction, converges to this new state with opposite up-down symmetry compared to the original plasma state. This observation is consistent with earlier SOLPS modelling of the DEMO-FNS CDN configuration [8]. The asymmetries presented in this paper are ultimately due to small imperfections in the initial asymmetry of the solutions, and their direction should not be interpreted as a true feature of the EU-DEMO CDN configuration. However, the results indicate an important feature of this configuration, namely the creation of strong asymmetries due to any small deviation from a perfectly symmetric DN configuration, as long as all divertor legs are not yet detached. In the operating space with detached divertor plasmas, the initial conditions and imperfections in the symmetry play only a minor role.

3.2. Changes to upstream profiles due to Ar seeding

Ar seeding influences both the fuelling efficiency and the steepness of the radial profiles of the main plasma parameters, see Fig. 6. The reduction in the fuelling efficiency appears to correlate with the target conditions: A close to linear dependence is obtained between Γ_D and the sum of the neutral pressures in the two divertors, as expected for our pumping scenario. At constant upstream density, the divertor neutral pressures (average values on the PFR rings furthest away from the X-points) are found to increase with Ar seeding, which is likely a result of increasing recycling at low seeding levels and both the ionization front moving away from the targets and reduction of the power available for ionization at higher seeding levels. This observation is consistent with recent ITER modelling [9].

The changes in the upstream radial profiles can be viewed to result from several mechanisms. As the core radiation losses are small, the power crossing the separatrix remains constant throughout the Ar seeding scan. Within a few λ_q distance from the separatrix, the SOL profiles are sensitive to the radiative power losses along the open field lines. As the power losses increase, faster heat flux decay is obtained in the radial direction, which reduces T_e in the SOL. On the core side, the density begins to increase as the ionization rate of neutrals on closed field lines exceeds the source rate of neutrals specified at the core boundary, leading to a steepening of the density profile and a simultaneous decrease in the core temperature. The core ionization source in-

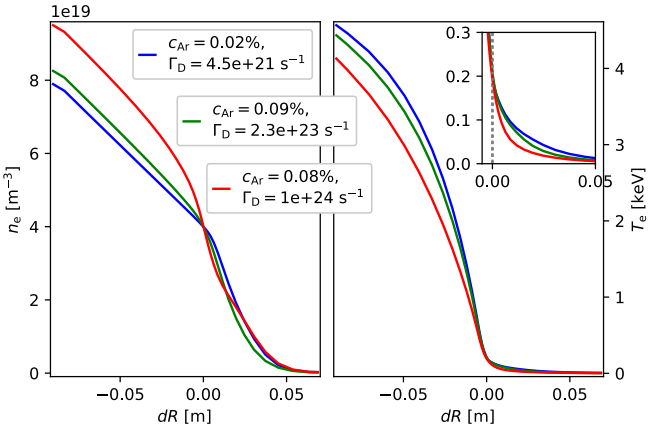

Fig. 6. Effects of Ar seeding on the radial profiles of n_e and T_e at the outer midplane. The three curves correspond to seeding rates $\Gamma_{Ar} = 3.5 \times 10^{18}$ s^{-1} (blue curve), $\Gamma_{Ar} = 1.4 \times 10^{20}$ s^{-1} (green curve), and $\Gamma_{Ar} = 4 \times 10^{20}$ s^{-1} (red curve). The Ar concentration, c_{Ar}, is evaluated as n_{Ar}/n_e on the last core ring just before the separatrix. (For interpretation of the references to colour in this figure legend, the reader is referred to the web version of this article.)

creases by almost a factor of 5 when entering the detached regime, explaining the large increase in core density for the case with the highest Ar seeding level.

3.3. Operating space in comparison to SN

Fig. 7 illustrates the operating spaces obtained in the simulations for the DN and for the SN configurations (a closely resembling EU-DEMO SN configuration has been previously analysed in [10]). In both configurations, the most critical target, on which T_e drops below 5 eV later than elsewhere with increasing seeding and fuelling, is the lower outer target. It is also true that when $T_{e,LO} < 5$ eV, the peak heat loads are below 10 MW/m^2 at all targets (facilitated by the choice of a shallow incidence angle). Therefore, it is sufficient to illustrate in Fig. 7 the evolution of $T_{e,LO}$ and the boundaries at which $T_{e,LO} = 5$ eV and $n_{sep,omp} = 0.6n_{GW}$. Solutions located between these two boundaries at the upper right corners of the figures are possible operating points, at least for the assumptions made in our present work.

Possible operating points can be identified in both the DN and the SN configurations, but the operating spaces do not appear to be very large. It is possible, that more stringent assumptions (e.g. a lower limit for $n_{sep,omp}$, narrower λ_q, higher P_{in}, larger incidence angle) or inclusion of additional terms in the analysis (e.g. additional heat loads due to photon transport, which was neglected here) could lead to closing of the operational space altogether (see also discussion about this in [10]). However, uncertainties in our assumptions also leave space for relaxing the exhaust requirements. Keeping this uncertainty in mind, we would like to see if by changing to a DN configuration we can obtain any more margin for possible operating points or otherwise more attractive conditions for reactor operation compared to the baseline SN configuration.

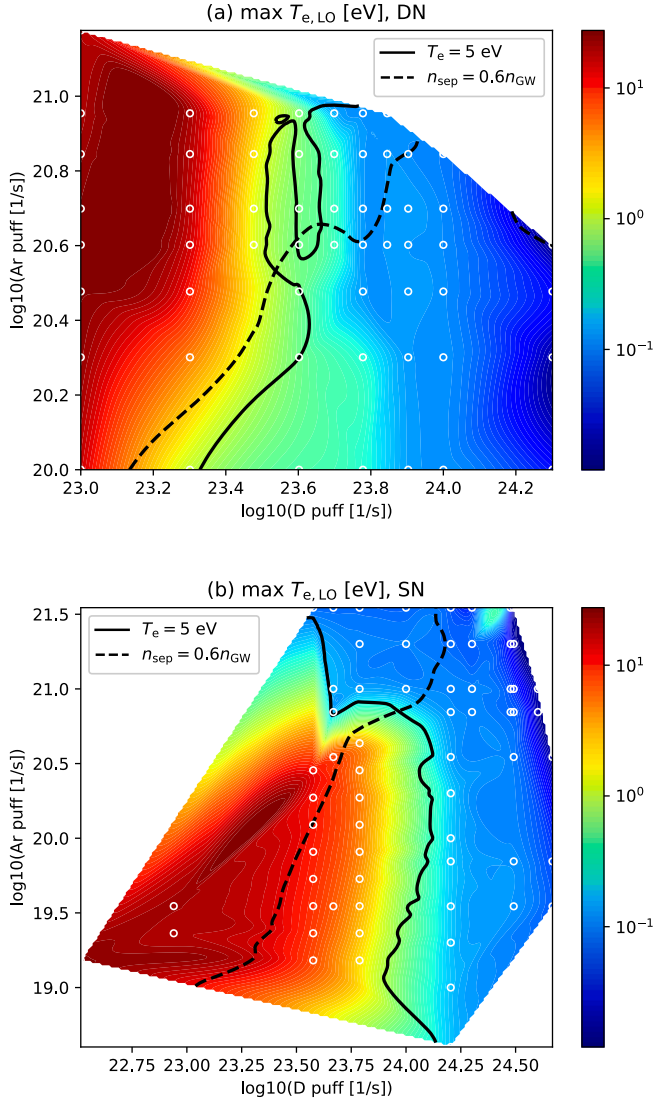

Fig. 7. Operating spaces in the DN and SN configurations.

As the absolute values of the puffing and seeding levels are highly sensitive to our assumptions on pumping and neutral model, and these have been simplified in the present work, one should not use the visible ranges of gas puff levels in Fig. 7 to directly compare the operating windows. The parametric dependencies shown in Fig. 8 are expected to give more reliable information about the properties of the possible operating spaces. In both configurations, Z_{eff} (average value on the simulated core flux surfaces) stays low, indicating that Ar can be considered as a very effective divertor and SOL radiator in EU-DEMO. The level of Z_{eff} is remarkably similar in both configurations, increasing towards the lower upstream densities. There are also no big differences in the radiated power fractions, and we see that $f_{rad,SOL}$ is above 70% for most of the operating points. Together with the assumption of 300 MW core radiation, this would imply a total radiated power fraction around 90% at least in both configurations.

Higher values of divertor neutral pressure are obtained in the SN configuration, but the He enrichment is higher in the DN configuration. The up-down asymmetry observed in the He enrichment in the DN configuration results from the asymmetric evolution of the plasma in the attached state, described in 3.1. With slightly different initial conditions, the asymmetry could be opposite, so one should only note that such an asymmetry is possible, but its direction is not fixed for the DN configuration. The absolute levels of the neutral pressure and He enrichment are likely to be sensitive to both the neutral model and the pumping model, but with our simplified picture we at least could not identify any major differences between the two configurations.

4. Discussion and conclusions

A DN configuration is considered as a possible alternative for the SN configuration in the EU-DEMO, with the hope that part of the critical power loading of the lower outer divertor could be shared by the upper divertor. Our simulations indicate that this indeed happens, as the lower outer divertor receives only ~ 30% of the SOL power, but it does not necessarily lead to lower requirements on the radiated power fraction or upstream density for safe operation. In our present study, we could not yet identify major improvements in the power exhaust that could widen the operational window for the EU-DEMO, when employing a symmetric DN configuration. In our paper we have drawn a first picture of the evolution of divertor conditions from the attached regime to the detached regime in the EU-DEMO CDN configuration. This does not constitute a full physics study of the configuration, but serves as an important basis for deciding and prioritizing more detailed future studies. Including the effects of both drifts and kinetic neutrals will increase the credibility of the solutions but, due to the observed tendence of the SOL plasma to create strong, metastable asymmetries in the attached cases, such studies should only be carried out for the detached regime identified in the present paper. Otherwise the possible effects of the additional physics could be easily overestimated as not all other small perturbations are included in the analysis. Seeding of other light impurities (N, Ne) might help broadening the radiation pattern in the SOL and divertors to cover larger temperature variations in the plasma, whereas seeding of heavier impurities will be needed to investigate the possible benefits of the DN configuration for core radiation.

Finally, it should be noted that a symmetric DN configuration is an ideal geometry, which in practice will always be realized as a disconnected DN configuration. This may lead to different power sharing between the four divertor legs compared to the symmetric DN, especially if the radial distance between the two separatrices cannot be kept very

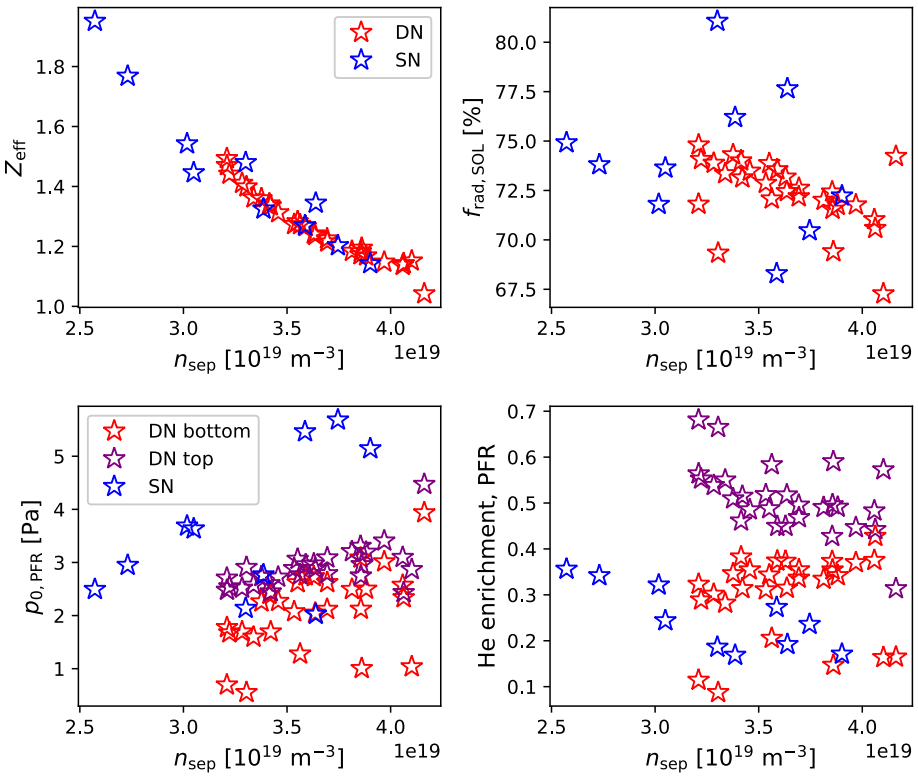

Fig. 8. Parametric dependencies within the operating spaces. Shown are Z_{eff} (top left), $f_{rad,SOL}$ (top right), neutral pressure in the PFR (bottom left) and He enrichment in the PFR (bottom right) as a function of $n_{sep,omp}$.

small.

CRediT authorship contribution statement

L. Aho-Mantila: Conceptualization, Methodology, Investigation, Writing - original draft, Visualization, Resources. **F. Subba:** Investigation, Validation, Resources. **D.P. Coster:** Conceptualization, Methodology, Software. **L. Xiang:** Validation, Resources, Software. **F. Militello:** Conceptualization, Methodology, Writing - review & editing, Project administration. **T. Lunt:** Conceptualization, Writing - review & editing, Resources. **D. Moulton:** Conceptualization, Writing - review & editing. **H. Reimerdes:** Conceptualization, Resources. **M. Wensing:** Validation, Resources. **M. Wischmeier:** Conceptualization, Writing - review & editing. **R. Ambrosino:** Resources. **X. Bonnin:** Software, Writing - review & editing. **M. Siccinio:** Conceptualization, Writing - review & editing.

Declaration of Competing Interest

The authors declare that they have no known competing financial interests or personal relationships that could have appeared to influence the work reported in this paper.

Acknowledgements

The work has received funding from the Academy of Finland (decision number 289726). This work has been carried out within the framework of the EUROfusion Consortium and has received funding from the Euratom research and training programme 2014–2018 and 2019–2020 under grant agreement No 633053. The views and opinions expressed herein do not necessarily reflect those of the European Commission, of the Academy of Finland, or of the ITER Organization.

References

[1] H. Reimerdes, et al., Nucl. Fusion 60 (6) (2020), https://doi.org/10.1088/1741-4326/ab8a6a, 066 030.
[2] F. Militello, L. Aho-Mantila, R. Ambrosino, T. Body, H. Bufferand, G. Calabro, G. Ciraolo, D. Coster, G. Di Gironimo, P. Fanelli, N. Fedorczak, A. Herrmann, P. Innocente, R. Kembleton, J. Lilburne, T. Lunt, D. Marzullo, S. Merriman, D. Moulton, A.H. Nielsen, J. Omotani, G. Ramogida, H. Reimerdes, M. Reinhart, P. Ricci, F. Riva, A. Stegmeir, F. Subba, W. Suttrop, P. Tamain, M. Teschke, A. Thrysoe, W. Treutterer, S. Varoutis, M. Wensing, A. Wilde, M. Wischmeier, L. Y. Xiang, Preliminary analysis of alternative divertors for DEMO, Nucl. Mate. Energy 26 (2021) 100908, https://doi.org/10.1016/j.nme.2021.100908. ISSN 2352-1791.
[3] D.P. Coster, Contrib. Plasma Phys. 56 (6–8) (2016) 790–795, https://doi.org/10.1002/ctpp.201610035.
[4] S. Wiesen, et al., J. Nucl. Mater. 463 (2015) 480–484. ISSN 0022–3115.https://doi.org/10.1016/j.jnucmat.2014.10.012. PLASMA-SURFACE INTERACTIONS 21.
[5] X. Bonnin, et al., Plasma Fusion Res. 11 (1403) (2016) 102.
[6] Coster D P et al, 2004 Physica Scripta 7. doi: 10.1238/physica.topical.108a00007.
[7] V. Rozhansky, et al., Nucl. Fusion 52(10) (2012) 103 017.https://doi.org/10.1088/0029-5515/52/10/103017.
[8] A.S. Kukushkin, S.I. Krasheninnikov, Plasma Phys. Control. Fusion 61 (074) (2019) 001, https://doi.org/10.1088/1361-6587/ab1bba.
[9] R. Pitts, et al., Nucl. Mater. Energy 20 (2019) 100 696. ISSN 2352-1791.https://doi.org/10.1016/j.nme.2019.100696.
[10] F. Subba, et al., Plasma Phys. Control. Fusion 60 (3) (2018), https://doi.org/10.1088/1361-6587/aaa508, 035 013.